Supporting Information For:

5,9-Dioxa-13b-Oxophosphanaphtho[3,2,1-*de*]anthracenes Prepared by Tandem Phospha-Friedel–Crafts Reaction as Hole-/Exciton-Blocking Materials for OLEDs

Soichiro Nakatsuka,[†] Hajime Gotoh,[†] Akiko Kageyama,[‡] Yasuyuki Sasada,[‡] Toshiaki Ikuta,[‡] Takuji Hatakeyama[*,†]

[†]Department of Chemistry, School of Science and Technology, Kwansei Gakuin University, 2-1 Gakuen, Sanda, Hyogo 669-1337, Japan

[‡]JNC Petrochemical Corporation, 5-1 Goi Kaigan, Ichihara, Chiba 290-8551, Japan

Table of Contents

A representative procedure for phospha-Friedel–Crafts reaction shown in Table 1

A solution of butyllithium in hexane (3.75 mL, 1.64 M, 6.0 mmol) was added slowly to a solution of 1,3-diphenoxybenzene **2** (1.31 g, 5.0 mmol) in benzene (15 mL) at 0 ºC under a nitrogen atmosphere. After stirring at 70 ºC for 4 h. Phosphorus trichloride (0.670 mL, 7.5 mmol) and S_8 (0.288 g, 9.0 mmol) was added slowly at 0 ºC. After the reaction mixture was reflux for 1 h, $AlCl_3$ and NEt^iPr_2 was added at 0 ºC. After stirring at reflux for 20 h, the reaction mixture was added to a solution of 1,4-diazabicyclo[2,2,2]octane (twice equivalents with respect to $AlCl_3$) in dichloromethane (500 ml), and filtered with a pad of Celite®. After the solvent was removed *in vacuo* to dryness, the crude product was dissolved in toluene and the residue was filtered off. After the solvent was condensed *in vacuo*, the yield of **3** in the crude product was determined by ^{1}H NMR analysis using dibromomethane as an internal standard.

Table S1. Screening of quantities of additives

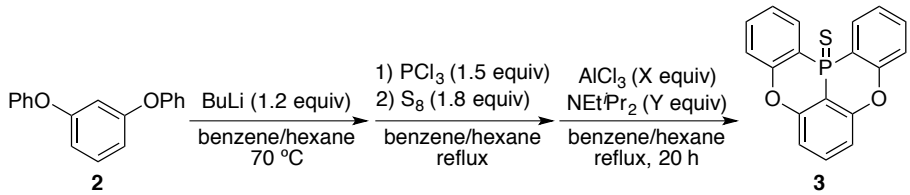

entry[a]	X	Y	yield[b] (%) of **3**
1	6.0	2.0	46%
2	7.0	2.0	51%
3	7.0	0	20%
4	7.0	1.0	36%
5	7.0	2.5	53%
6	7.0	3.0	49%

[a]Reactions were carried out on a 5.0 mmol scale. [b]Determined by ^{1}H NMR analysis using dibromomethane as an internal standard.

Crystallographic Data.

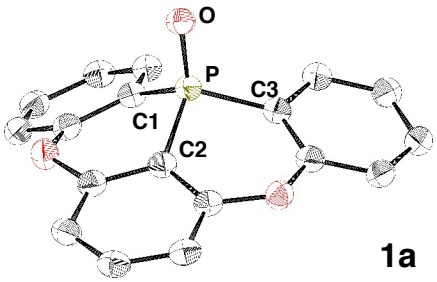

Selected bond lengths
P–O 1.4889(11) Å
P–C1 1.7897(16) Å
P–C2 1.7677(16) Å
P–C3 1.7859(16) Å

Selected angles
C1–P–C2 98.78(7)°
C2–P–C3 99.44(7)°
C1–P–C3 114.50(7)°

Formula	$C_{18}H_{11}O_3P$
Formula Weight	306.24
Temperature, K	100(2)
Wavelength, Å	0.85000
Crystal System	Triclinic
Space Group	P–1 (No. 2)
a, Å	8.02200(10)
b, Å	8.48070(10)
c, Å	10.8128(2)
α, deg	87.5127(5)
β, deg	70.3489(6)
γ, deg	73.5142(9)
Volume, Å	663.191(17)
Z	2
Density_{calcd}, g·cm^{-3}	1.534

Abs. Coefficient, cm^{-1}	0.346
F(000)	316
Crystal Size, mm^3	0.10, 0.10, 0.10
$2\theta_{min}$, $2\theta_{max}$, deg	6.82, 63.00
Index Ranges	–9≤h≤9
	–10≤k≤10
	–13≤l≤13
Reflections (unique)	2502
Reflections (I>2.0σ(I))	2459
Parameters	200
GOF on F^2	1.071
$R1$ (I>2.0σ(I))	0.0427
R, w$R2$ (all data)	0.0430, 0.1168
Largest diff peak and hole, e, Å^{-3}	0.346, –0.396

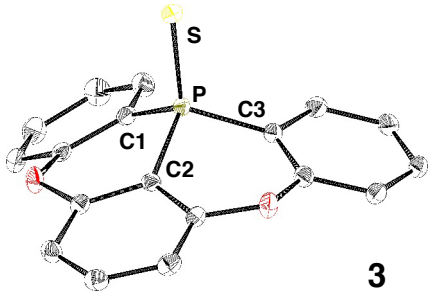

Selected bond lengths
P–S 1.9568(6) Å
P–C1 1.7929(16) Å
P–C2 1.7720(16) Å
P–C3 1.7929(16) Å

Selected angles
C1–P–C2 99.19(7)°
C2–P–C3 99.05(7)°
C1–P–C3 114.61(8)°

Formula	$C_{18}H_{11}O_2PS$
Formula Weight	322.30
Temperature, K	100(2)
Wavelength, Å	0.85000
Crystal System	Monoclinic
Space Group	$P\,2_1/a$ (No. 14)
a, Å	8.19170(10)
b, Å	20.1049(2)
c, Å	8.93790(10)
β, deg	103.1295(3)
Volume, Å	1433.53(3)
Z	4
Density_{calcd}, g·cm^{-3}	1.493

Abs. Coefficient, cm^{-1}	0.551
F(000)	664
Crystal Size, mm^3	0.10, 0.10, 0.10
$2\theta_{min}$, $2\theta_{max}$, deg	6.10, 63.00
Index Ranges	–10≤h≤10
	–24≤k≤24
	–10≤l≤10
Reflections (unique)	2685
Reflections (I>2.0σ(I))	2606
Parameters	199
GOF on F^2	1.050
$R1$ (I>2.0σ(I))	0.0350
R, w$R2$ (all data)	0.0357, 0.0941
Largest diff peak and hole, e, Å^{-3}	0.446, –0.421

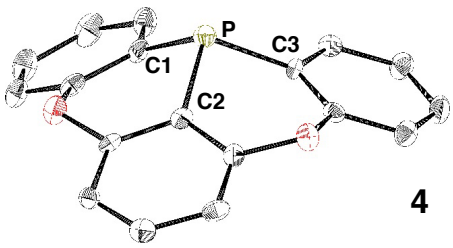

Selected bond lengths
P–C1 1.834(4) Å
P–C2 1.813(4) Å
P–C3 1.832(4) Å

Selected angles
C1–P–C2 95.30(19)°
C2–P–C3 96.02(18)°
C1–P–C3 109.4(2)°

Formula	$C_{18}H_{11}O_2P$
Formula Weight	290.24
Temperature, K	100(2)
Wavelength, Å	0.71075
Crystal System	Monoclinic
Space Group	$P\,2_1/c$ (No. 14)
a, Å	9.200(3)
b, Å	10.920(3)
c, Å	13.430(4)
β, deg	88.087(13)
Volume, Å	1348.5(7)
Z	4
Density_{calcd}, g·cm^{-3}	1.430

Abs. Coefficient, cm^{-1}	0.204
F(000)	600
Crystal Size, mm^3	0.2, 0.2, 0.2
$2\theta_{min}$, $2\theta_{max}$, deg	6.08, 52.00
Index Ranges	–11≤h≤10
	–13≤k≤10
	–12≤l≤16
Reflections (unique)	2654
Reflections (I>2.0σ(I))	1425
Parameters	190
GOF on F^2	1.100
$R1$ (I>2.0σ(I))	0.0718
R, w$R2$ (all data)	0.1553, 0.1218
Largest diff peak and hole, e, Å^{-3}	0.343, –0.442

Figure S1. X-ray crystal structures of **1a**, **3** and **4** (left), and crystal data and structure refinements (right). Thermal ellipsoids are shown at 50% probability; hydrogen atoms have been omitted for clarity.

Computational studies. Molecular orbital calculations and nucleus-independent chemical shift (NICS) calculations were performed with Gaussian 09[1] packages. The DFT method was employed using the B3LYP hybrid functional.[2] Structures were optimized with the 6-31G(d) basis set.[3] Nucleus independent chemical shifts (NICS) were evaluated by using the gauge invariant atomic orbital[4] (GIAO) approach at the GIAO-B3LYP/6-31G(d) level. The electronic coupling calculations of dimers in the X-ray crystal structures were performed by the local density functional VWN in the conjunction with the PW91[5] gradient corrections with the DZP basis set,[6] as implemented in the ADF program[7] according to the literature.[8]

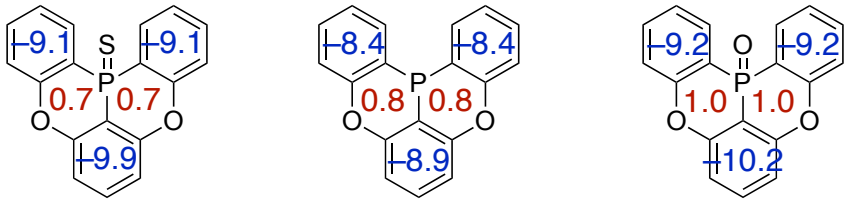

Figure S2. NICS(0) values of **1a**, **3** and **4** at the GIAO-B3LYP/6-311+G(d,p) level on Gaussian 09 program.

---

(1) Gaussian 09, Revision B.01, Frisch, M. J.; Trucks, G. W.; Schlegel, H. B.; Scuseria, G. E.; Robb, M. A.; Cheeseman, J. R.; Scalmani, G.; Barone, V.; Mennucci, B.; Petersson, G. A.; Nakatsuji, H.; Caricato, M.; Li, X.; Hratchian, H. P.; Izmaylov, A. F.; Bloino, J.; Zheng, G.; Sonnenberg, J. L.; Hada, M.; Ehara, M.; Toyota, K.; Fukuda, R.; Hasegawa, J.; Ishida, M.; Nakajima, T.; Honda, Y.; Kitao, O.; Nakai, H.; Vreven, T.; Montgomery, Jr., J. A.; Peralta, J. E.; Ogliaro, F.; Bearpark, M.; Heyd, J. J.; Brothers, E.; Kudin, K. N.; Staroverov, V. N.; Kobayashi, R.; Normand, J.; Raghavachari, K.; Rendell, A.; Burant, J. C.; Iyengar, S. S.; Tomasi, J.; Cossi, M.; Rega, N.; Millam, N. J.; Klene, M.; Knox, J. E.; Cross, J. B.; Bakken, V.; Adamo, C.; Jaramillo, J.; Gomperts, R.; Stratmann, R. E.; Yazyev, O.; Austin, A. J.; Cammi, R.; Pomelli, C.; Ochterski, J. W.; Martin, R. L.; Morokuma, K.; Zakrzewski, V. G.; Voth, G. A.; Salvador, P.; Dannenberg, J. J.; Dapprich, S.; Daniels, A. D.; Farkas, Ö.; Foresman, J. B.; Ortiz, J. V.; Cioslowski, J.; Fox, D. J. Gaussian, Inc., Wallingford CT, 2009.

(2) (a) Becke, A. D. *J. Chem. Phys.* **1993,** *98*, 5648–5652. (b) Lee, C.; Yang, W.; Parr, R. G. *Phys. Rev. B* **1988,** *37*, 785–789.

(3) Hehre, W. J.; Radom, L.; Schleyer, P. v. R.; Pople, J. A. *Ab Initio Molecular Orbital Theory*; John Wiley & Sons: New York, **1986** and references cited therein.

(4) (a) Dichtfield, R. *Mol. Phys.* **1974,** *27*, 789–807. (b) Wolinski, K.; Hinton, J. F.; Pulay, P. *J. Am. Chem. Soc.* **1990,** *112*, 8251–8260.

(5) Perdew, J. P.; Chevary, J. A.; Vosko, S. H.; Jackson, K. A.; Pederson, M. R.; Sing, D. J.; Fiolhais, C. *Phys. Rev. B* **1992,** *46*, 6671–6687.

(6) Lenthe, E. v.; Baerends, E. J. *J. Comput. Chem.* **2003**, *24*, 1142–1156.

(7) (a) Velde, G. t.; Bickelhaupt, F. M.; Gisbergen, S. J. A. v.; Fonseca Guerra, C.; Baerends, E. J.; Snijders J. G.; Ziegler, T. *J. Comput. Chem.* **2001**, *22*, 931–967. (b) Fonseca Guerra, C.; Snijders, J. G.; Velde, G. t.; Baerends, E. J. *Theor. Chem. Acc.* **1998**, *99*, 391–403. (c) ADF2010, SCM, Theoretical Chemistry, Vrije Universiteit, Amsterdam, The Netherlands.

(8) (a) Senthilkumar, K.; Grozema, F. C.; Bickelhaupt, F. M.; Siebbeles, L. D. A. *J. Chem. Phys.* **2003**, *119*, 9809–9817. (b) Wen, S.-H.; Li, A.; Song, J.; Deng, W.-Q.; Han, K.-L.; Goddard III, W. A. *J. Phys. Chem. B* **2009**, *113*, 8813–8819.

Table S2. Summary of TD-DFT calculation for 1a–c at the B3LYP/6-311+G(d,p)//B3LYP /6-31G(d) level.

compound	transition	wavelength (nm)	energy (eV)	oscillator strength	coefficient of HOMO–LUMO
1a	S_0–S_1	304.06	4.0776	0.1096	0.68892
	S_0–T_1	354.79	3.4945	0.0000	–
1b	S_0–S_1	318.39	3.8941	0.1025	0.69094
	S_0–T_1	389.41	3.1839	0.0000	–
1c	S_0–S_1	309.58	4.0050	0.1790	0.68914
	S_0–T_1	380.48	3.2587	0.0000	–

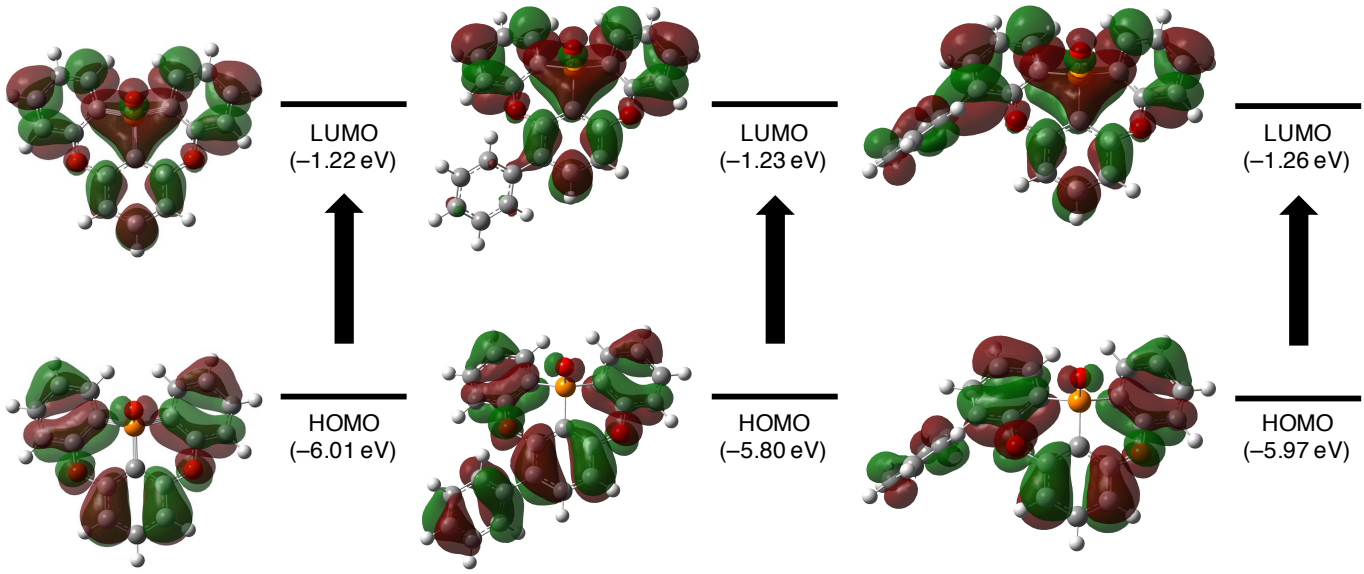

Figure S3. The highest occupied and lowest-unoccupied Kohn–Sham orbitals of **1a–c** in the S_0 state calculated at the B3LYP/6-31G(d) level (isovalue = 0.02). Orbital energies are shown in parentheses.

Photoluminescence spectroscopy. UV-visible absorption spectra of **1a**–**1c**, **3** and **4** (0.02 mM in $CHCl_3$ or CH_2Cl_2) were measured by UV-2600 (Shimadzu) and V-560 (JASCO Co.). PL spectra of **1a**–**1c**, **3** and **4** (0.02 mM in $CHCl_3$ or CH_2Cl_2) were measured by F-7000 (Hitachi High-Tech Co.) and FluoroMax-4P (HORIBA, Ltd.) at 298 K (fluorescence). Phosphorescence spectra (delayed component of PL spectra) of **1a**, **3** and **4** (saturated in 3-methylpentane) were measured by FluoroMax-4P at 77 K (liquid N_2).

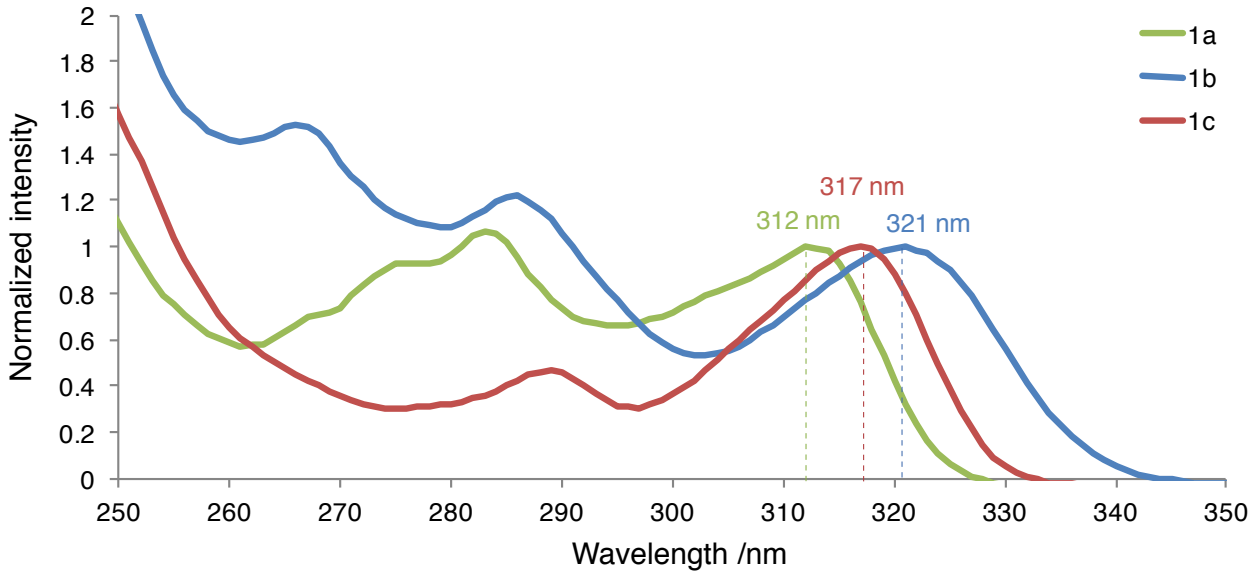

Figure S4. UV-visible absorption spectra of **1a** (green line), **1b** (blue line) and **1c** (red line) in $CHCl_3$ (0.02 mM solution) at 298 K.

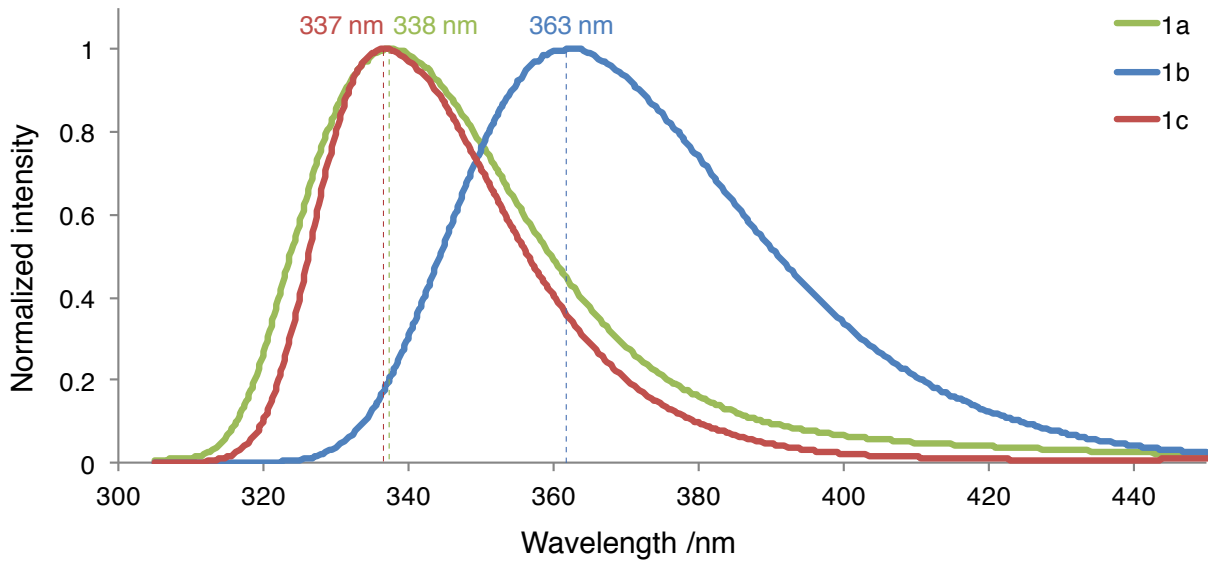

Figure S5. UV-visible absorption spectra of **1a** (green line, excitation at 280 nm), **1b** (blue line, excitation at 285 nm) and **1c** (red line, excitation at 290 nm) in $CHCl_3$ (0.02 mM solution) at 298 K.

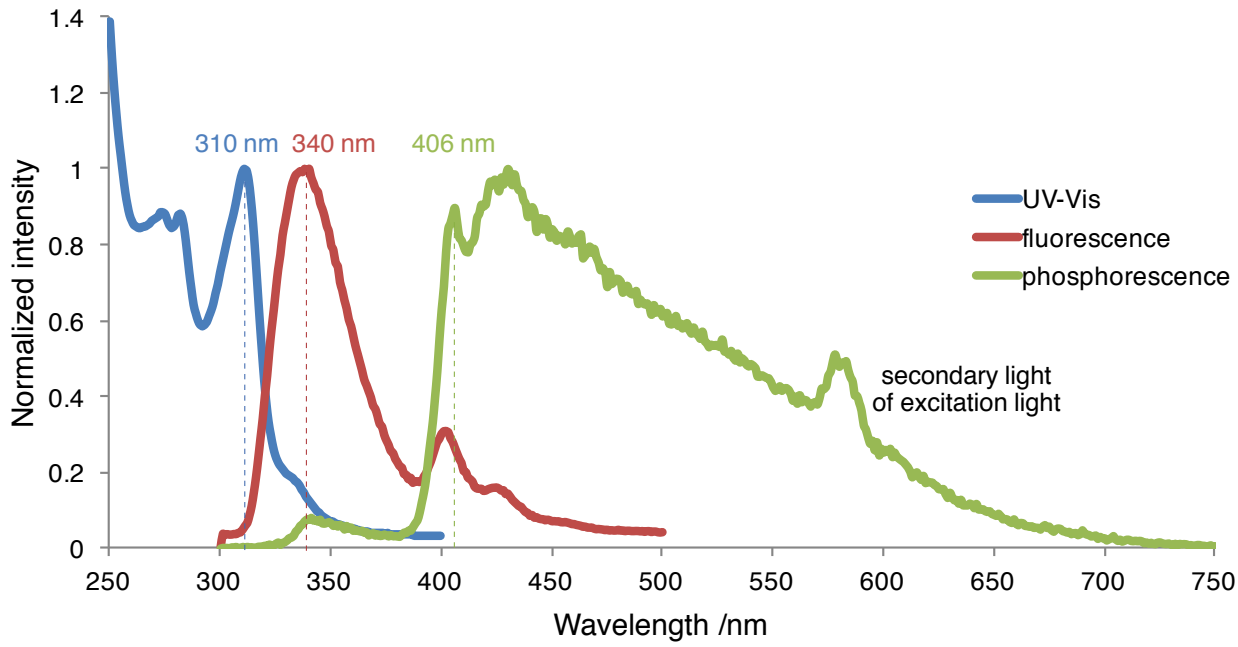

Figure S6. Normalized absorption (blue, 0.02 mM, CH_2Cl_2), fluorescence (red, 0.02 mM, CH_2Cl_2, excitation at 290 nm), and phosphorescence (green, saturated 3-methylpentane solution at 77 K, excitation at 290 nm) spectra of **1a**.

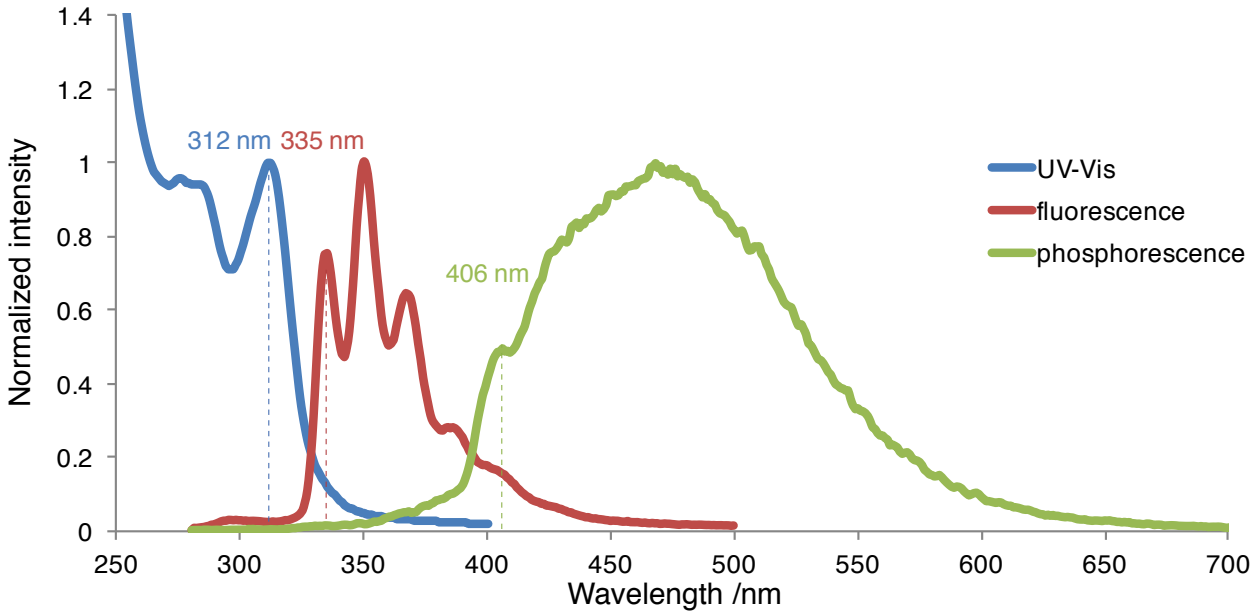

Figure S7. Normalized UV-visible absorption (blue, 0.02 mM, CH_2Cl_2), fluorescence (red, 0.02 mM, CH_2Cl_2, excitation at 270 nm), and phosphorescence (green, saturated 3-methylpentane solution at 77 K, excitation at 290 nm) spectra of **3**.

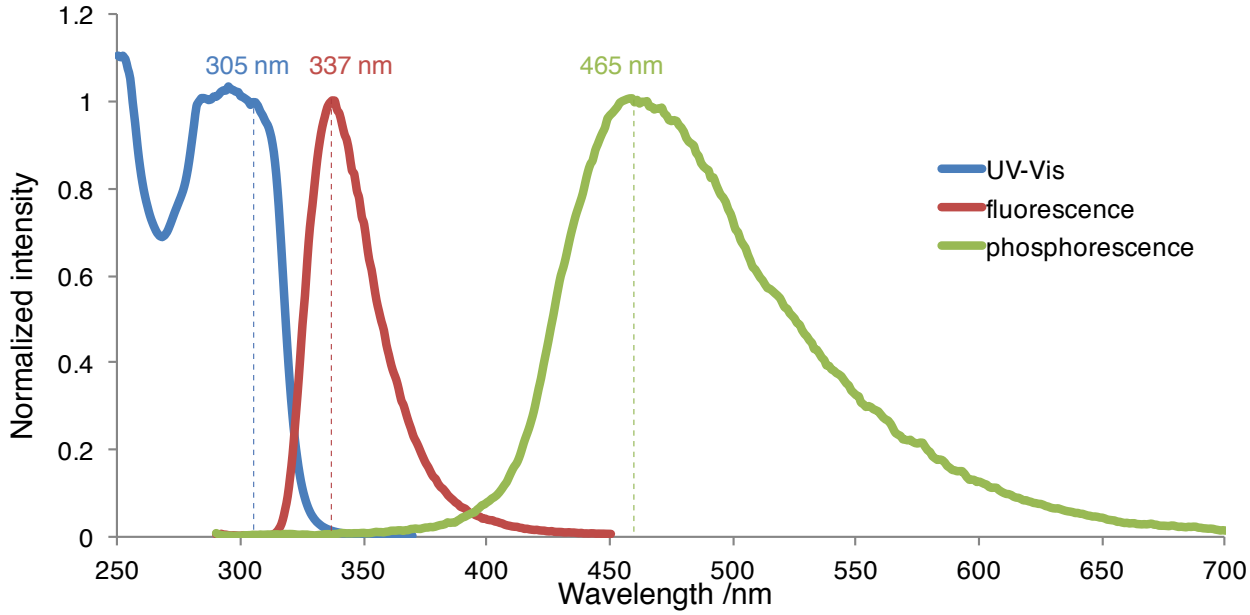

Figure S8. Normalized absorption (blue, 0.02 mM, CH_2Cl_2), fluorescence (red, 0.02 mM, CH_2Cl_2, excitation at 280 nm), and phosphorescence (green, saturated 3-methylpentane solution at 77 K, excitation at 280 nm) spectra of **4**.

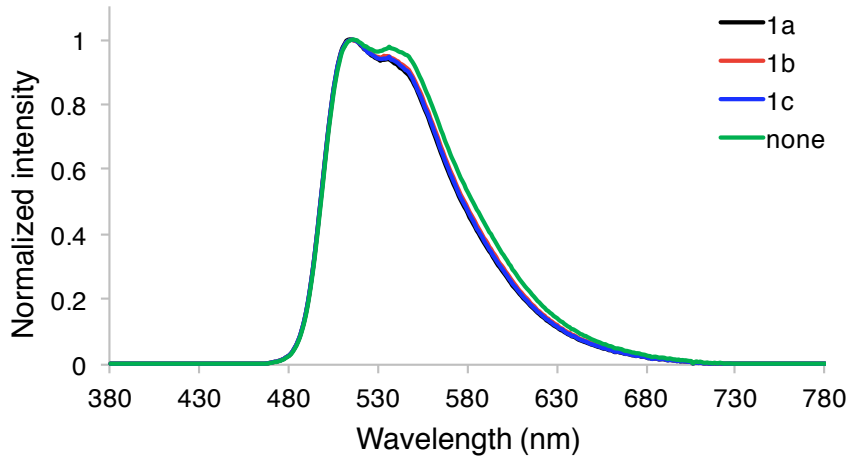

Figure S9. EL spectra of PHOLEDs using **1a** (black line), **1b** (red line) or **1c** (blue line) as a hole blocking material at 1000 cd m^{-2} at 298 K.

Measurement of cyclic voltammograms. Cyclic and differential pulse voltammetries were conducted on a BAS Electrochemical Analyzer ALS 604E and CS-3A using a three-electrode cell with a glassy carbon working electrode, a platinum wire counter electrode, and an $Ag/AgNO_3$ reference electrode.

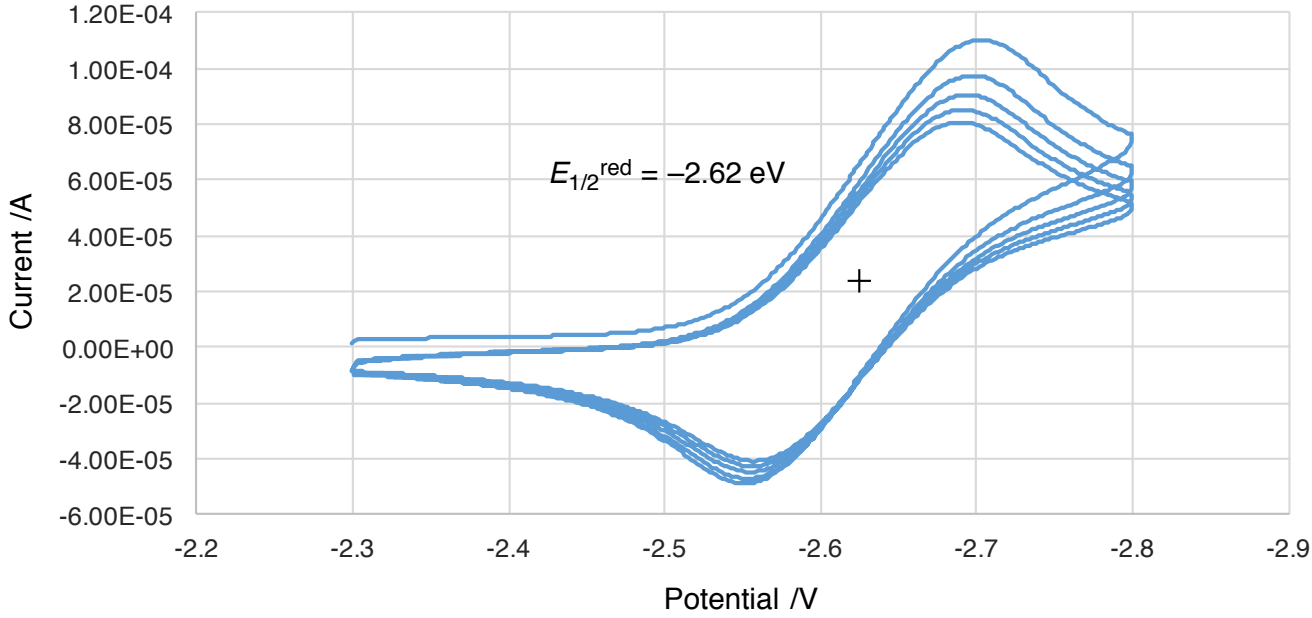

Figure S10. Cyclic voltammograms of (a) **1a**. Redox potentials were determined 2.0 mM in *N*,*N*-dimethylformamide (reduction) with 0.10 M $n\text{-}Bu_4N^+PF_6^-$ and given in V versus the ferrocene/ferrocenium couple (Fc/Fc^+).

^{1}H, ^{13}C and ^{31}P NMR spectra for isolated compounds

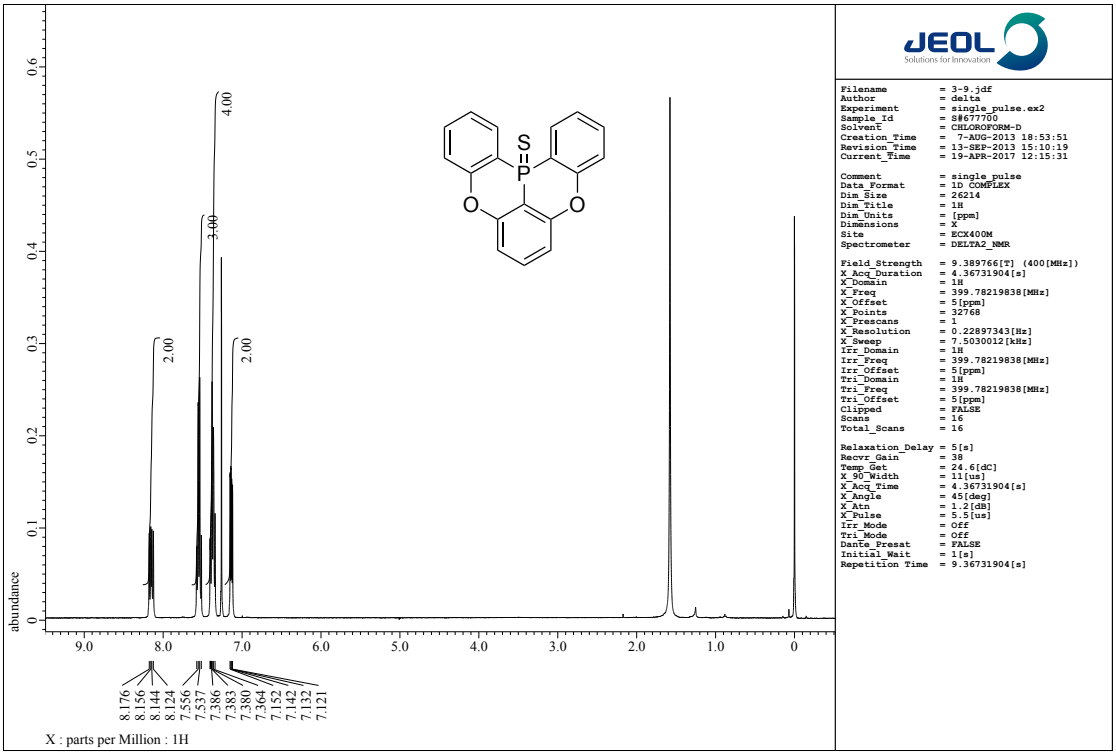

Figure S11. ^{1}H NMR spectrum of **3** in $CDCl_3$ at 25 °C.

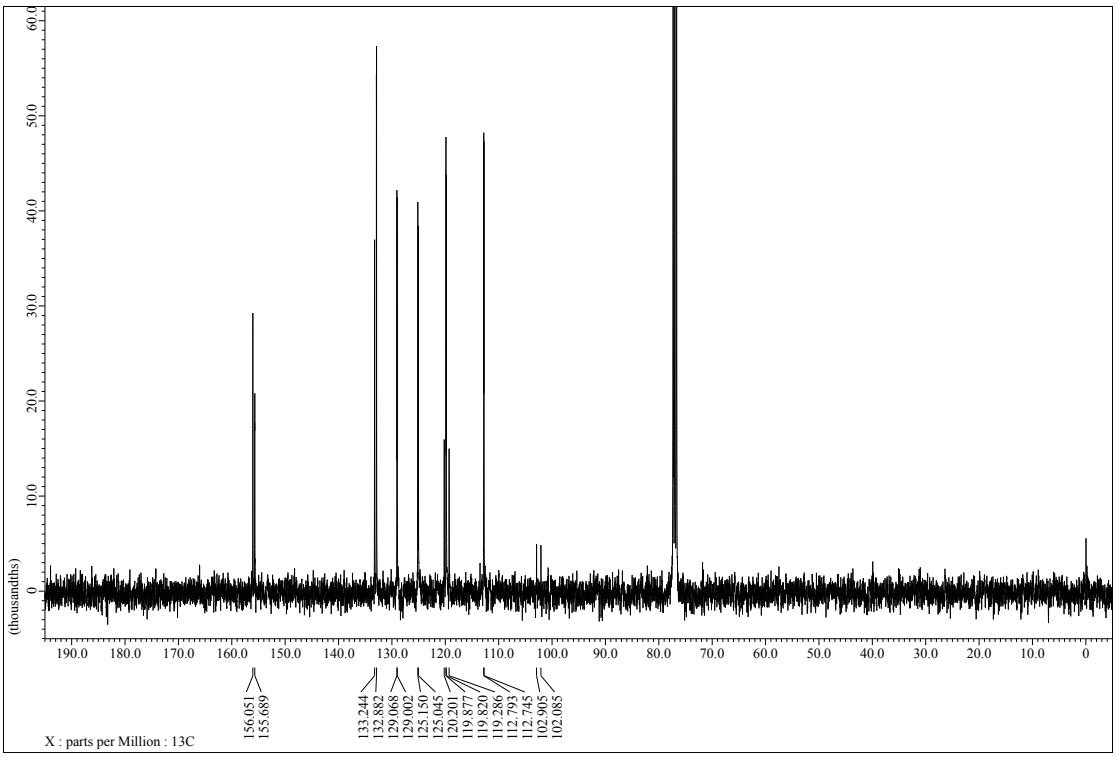

Figure S12. ^{13}C NMR spectrum of **3** in $CDCl_3$ at 25 °C.

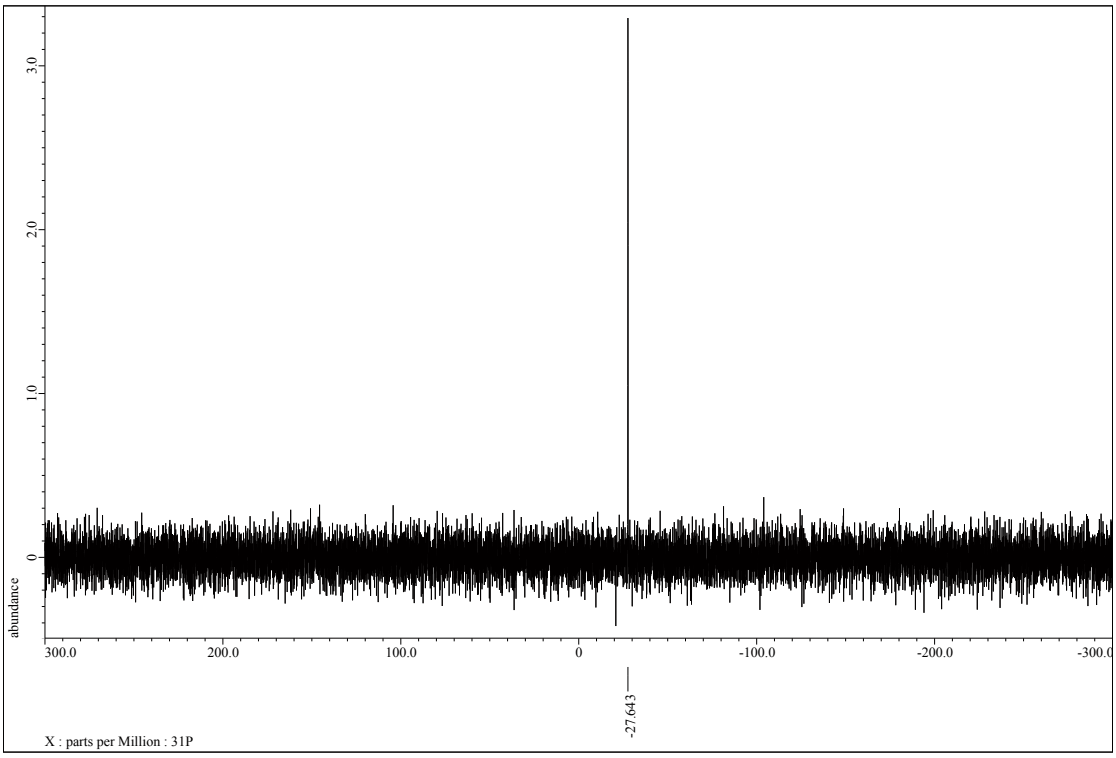

Figure S13. ^{31}P NMR spectrum of **3** in $CDCl_3$ at 25 °C.

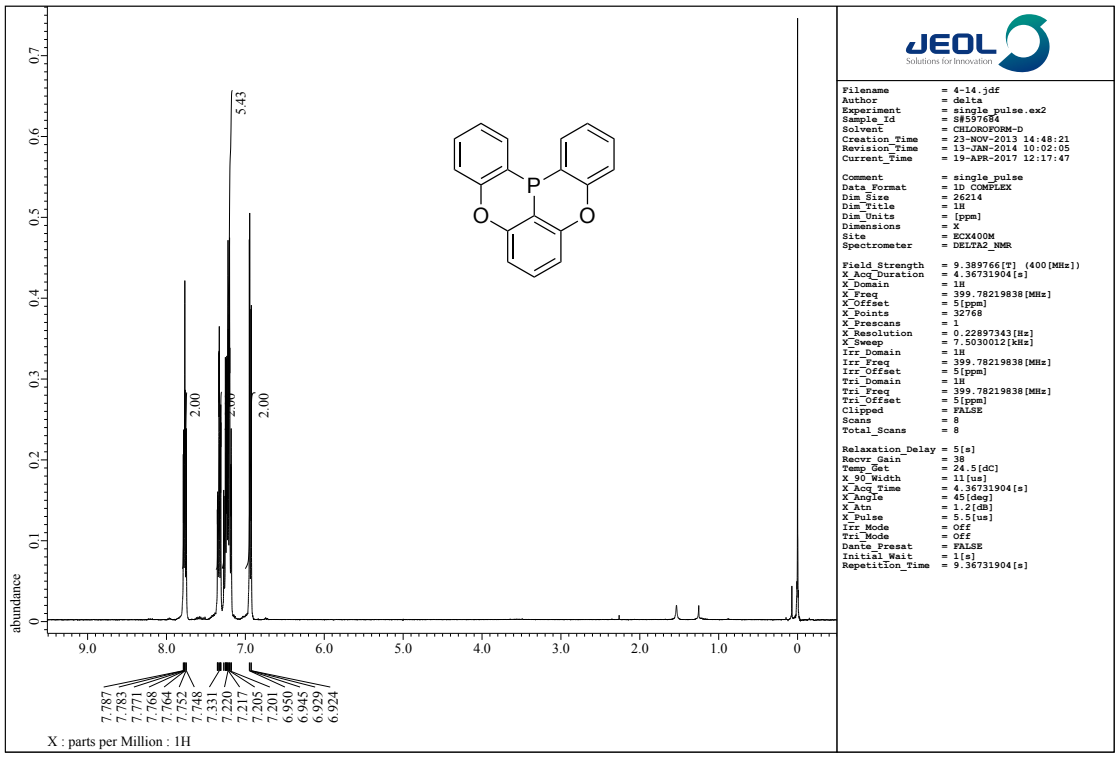

Figure S14. ^{1}H NMR spectrum of **4** in $CDCl_3$ at 25 °C.

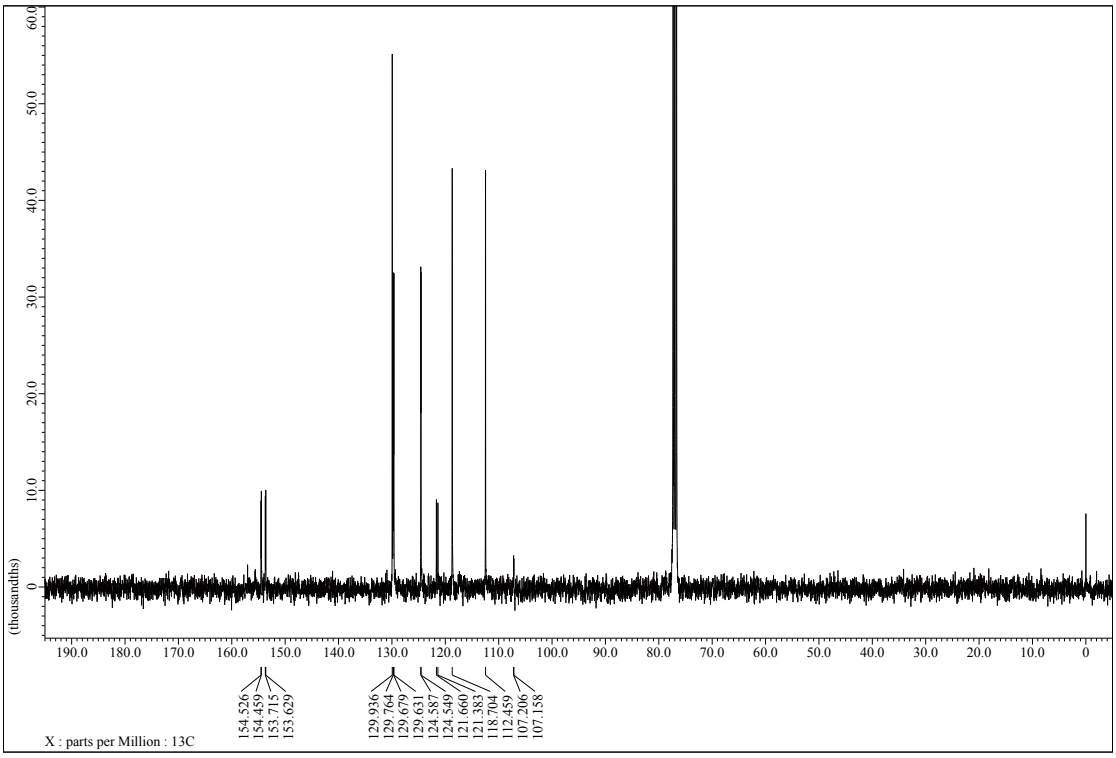

Figure S15. ^{13}C NMR spectrum of **4** in $CDCl_3$ at 25 °C.

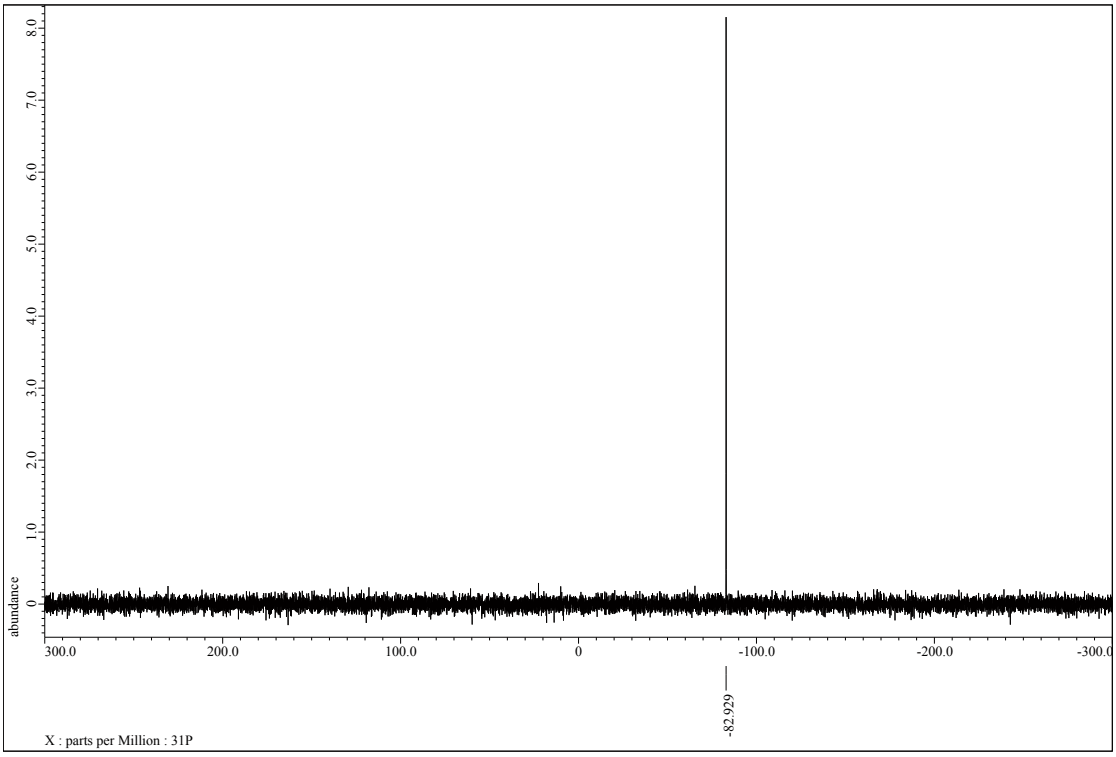

Figure S16. ^{31}P NMR spectrum of **4** in $CDCl_3$ at 25 °C.

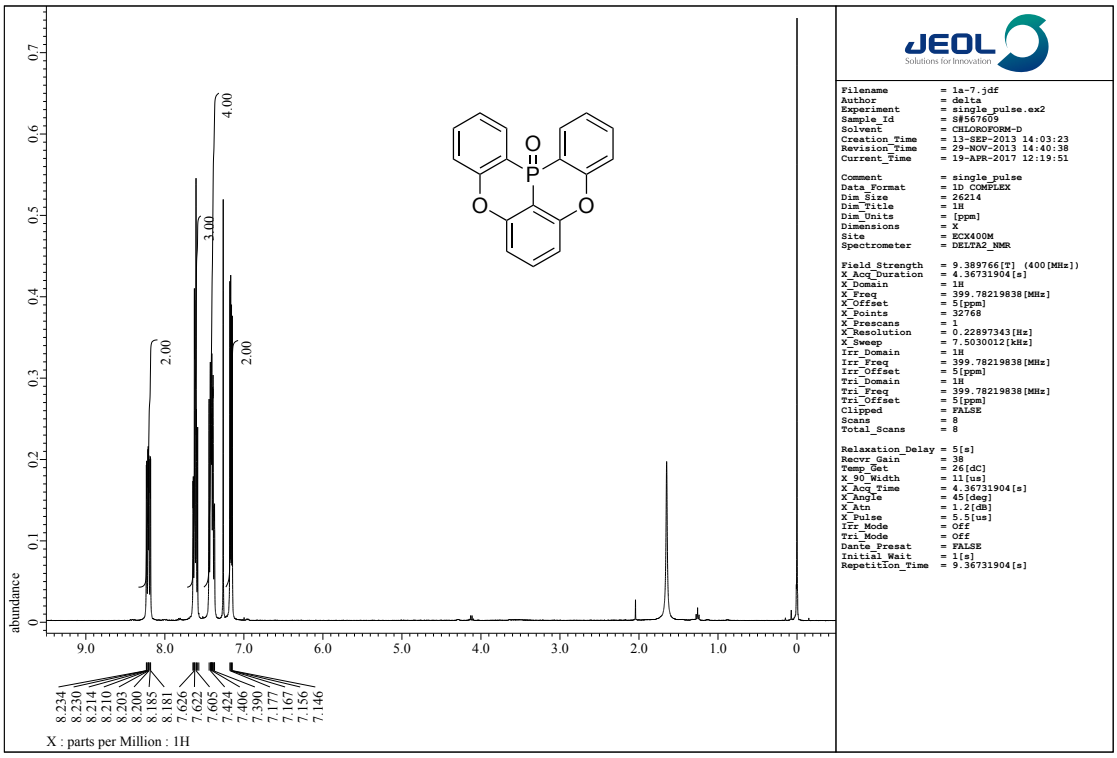

Figure S17. ^{1}H NMR spectrum of **1a** in $CDCl_3$ at 25 °C.

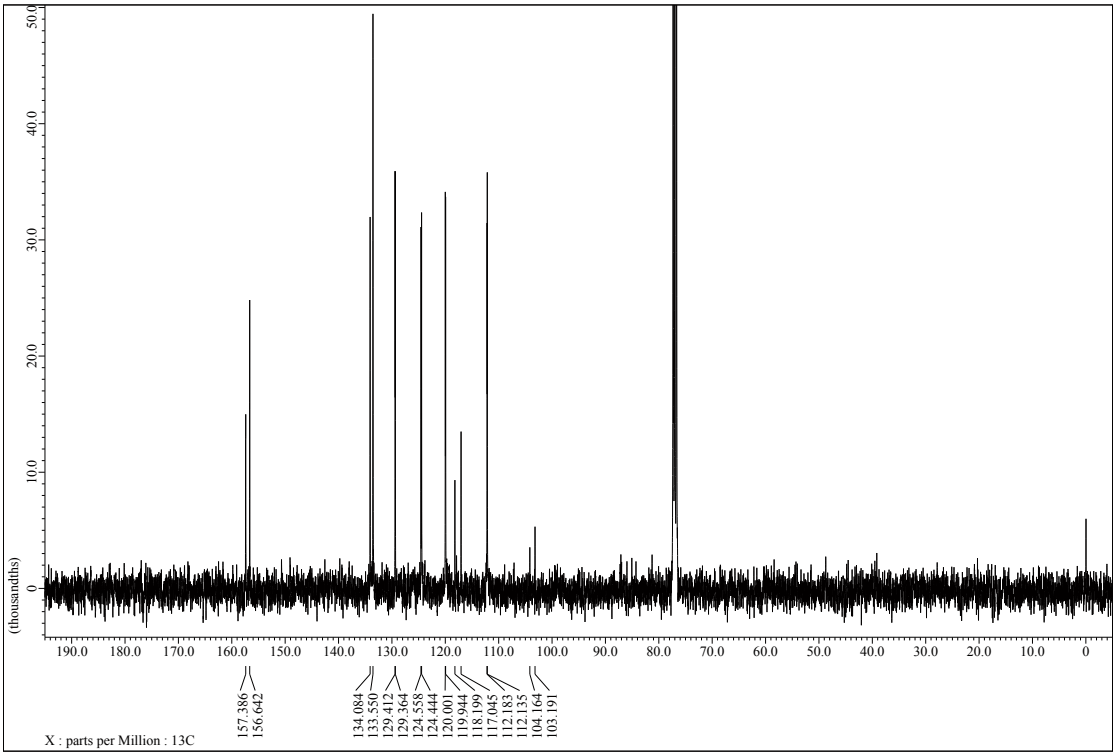

Figure S18. ^{13}C NMR spectrum of **1a** in $CDCl_3$ at 25 °C.

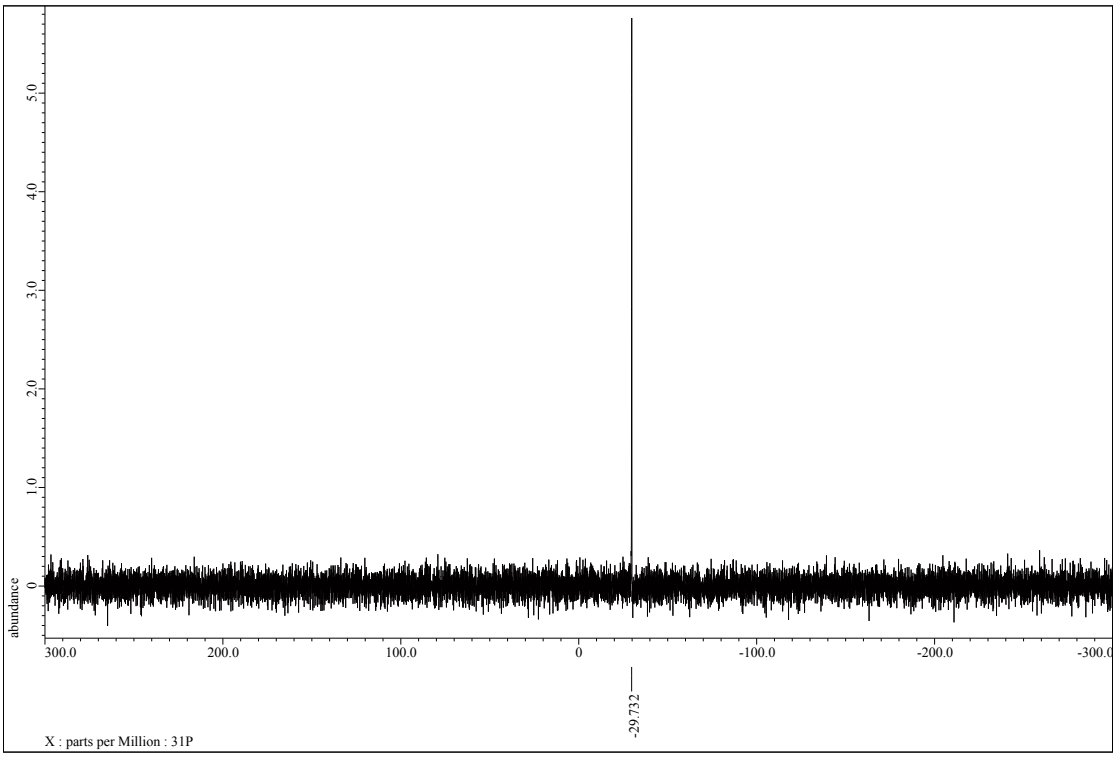

Figure S19. ^{31}P NMR spectrum of **1a** in $CDCl_3$ at 25 °C.

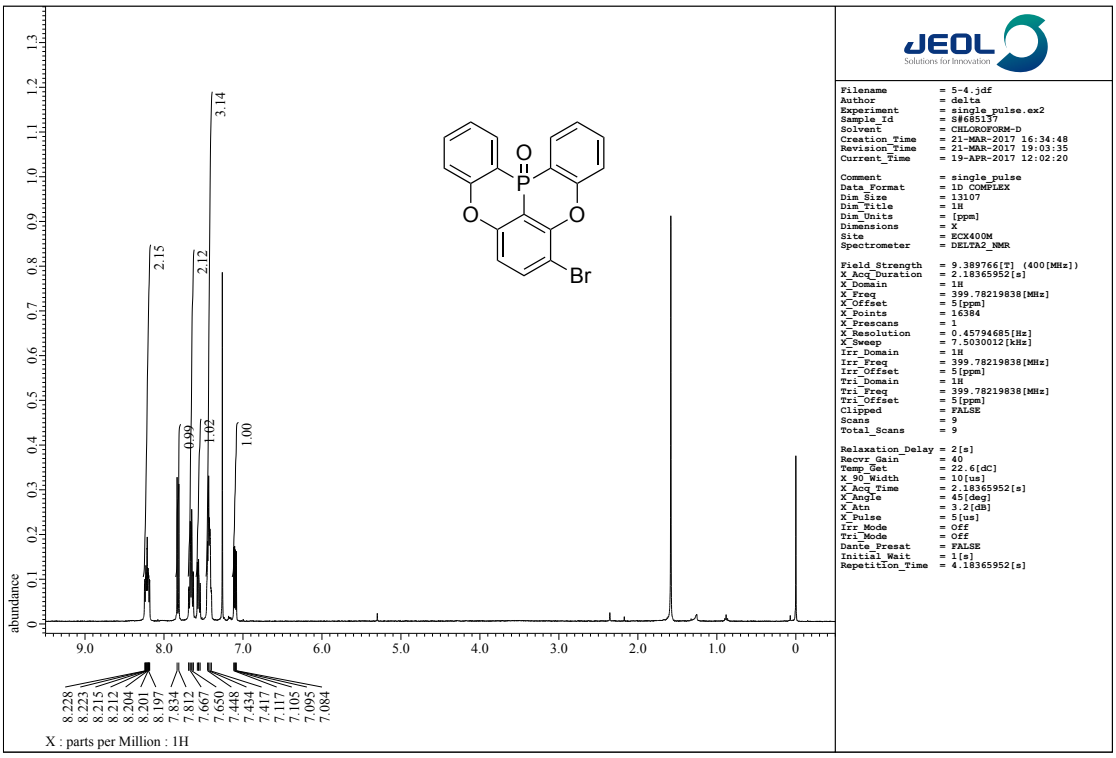

Figure S20. ^{1}H NMR spectrum of **5** in $CDCl_3$ at 25 °C.

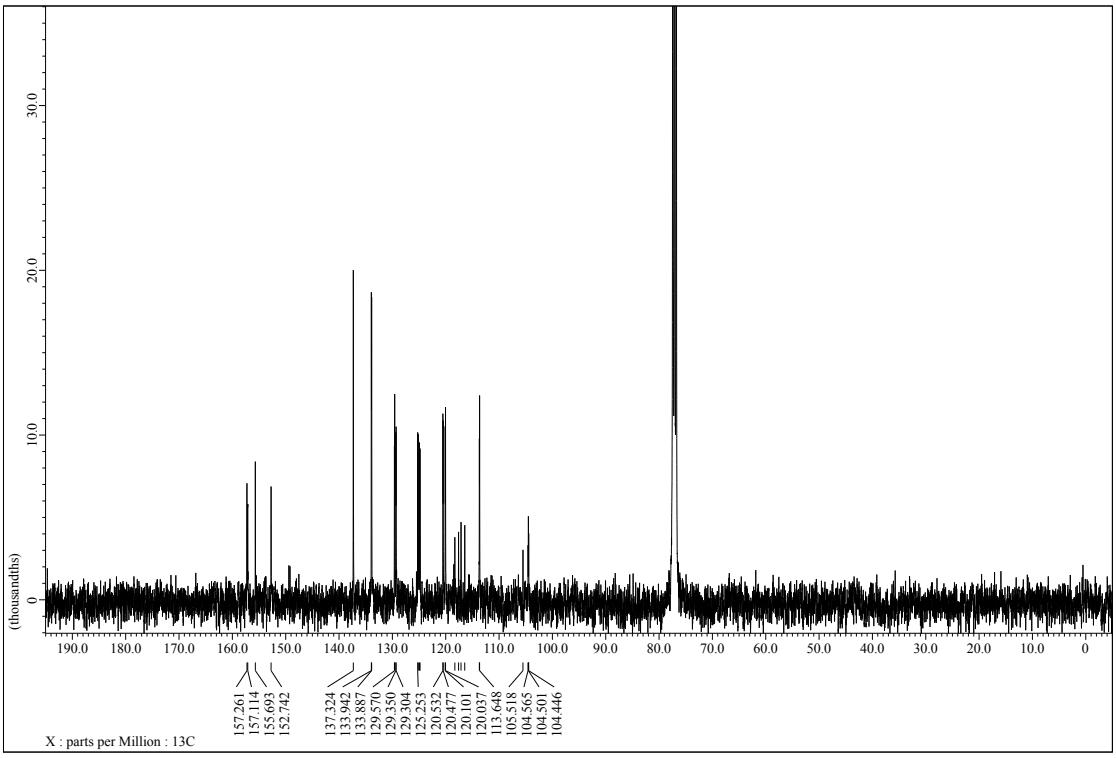

Figure S21. ^{13}C NMR spectrum of **5** in $CDCl_3$ at 25 °C.

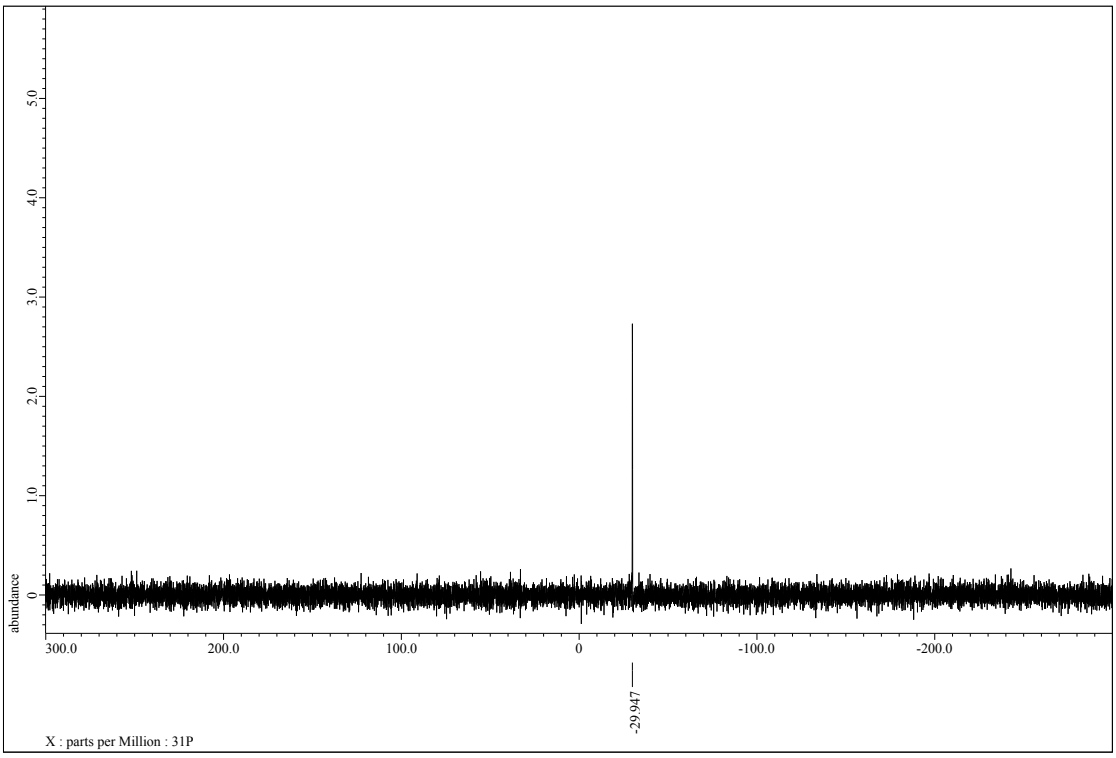

Figure S22. ^{31}P NMR spectrum of **5** in $CDCl_3$ at 25 °C.

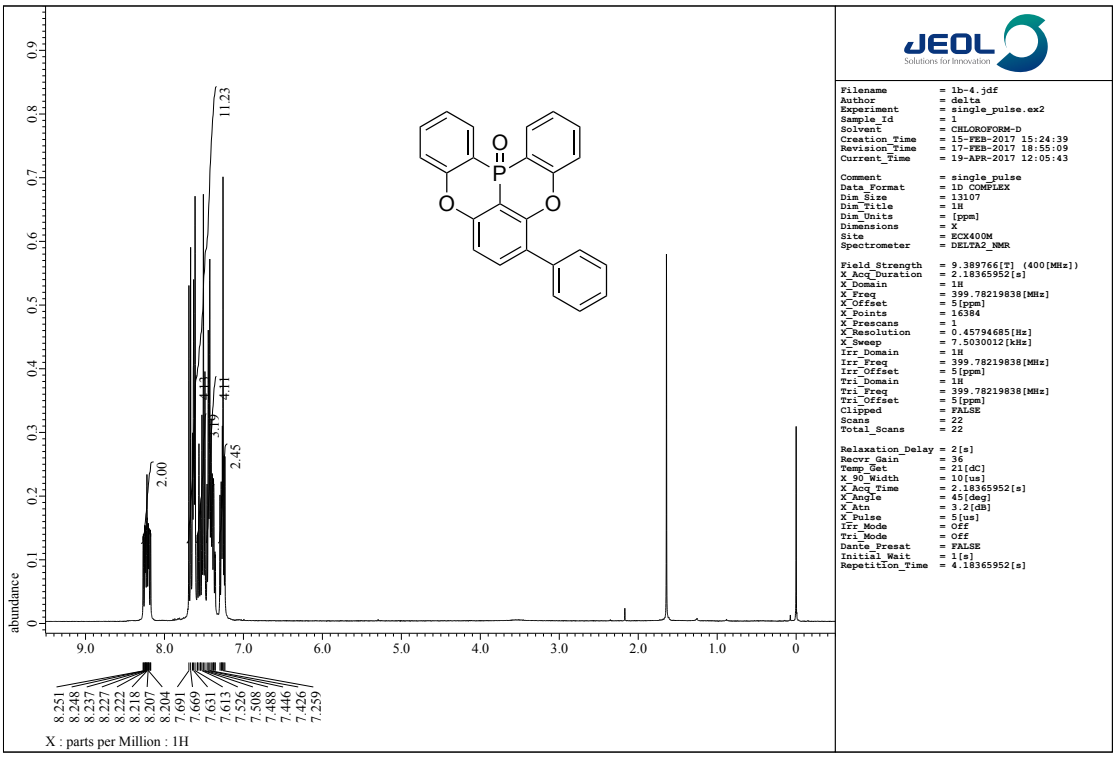

Figure S23. ^{1}H NMR spectrum of **1b** in $CDCl_3$ at 25 °C.

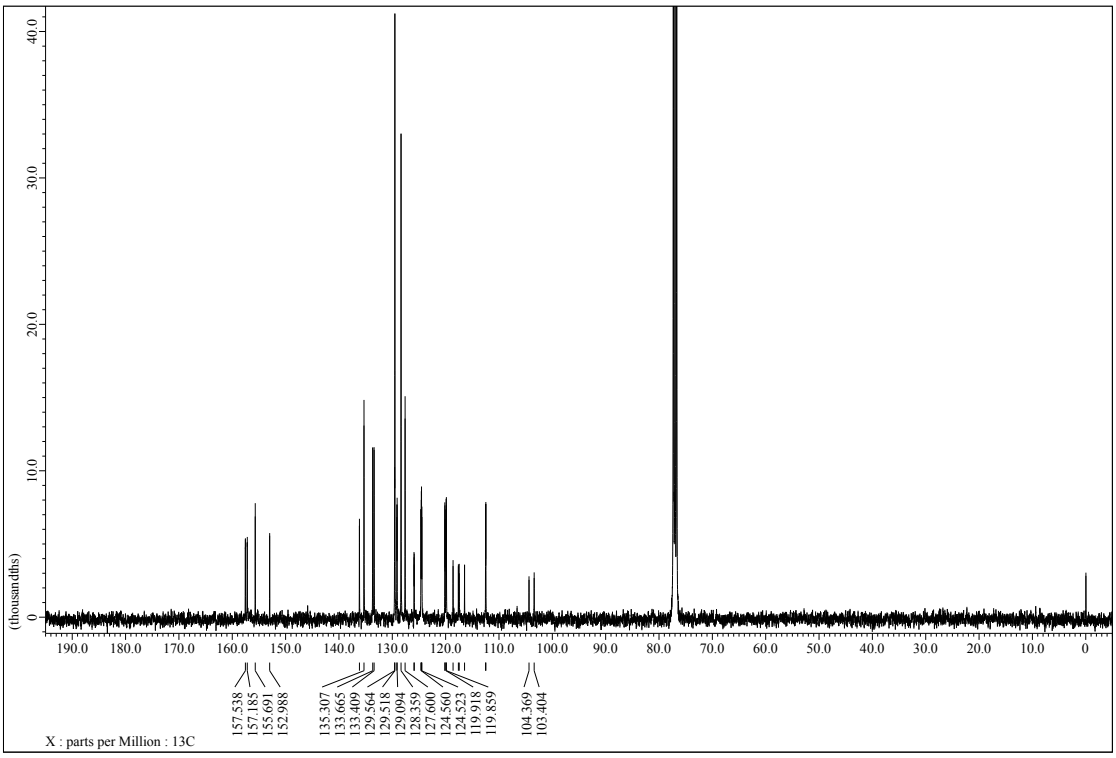

Figure S24. ^{13}C NMR spectrum of **1b** in $CDCl_3$ at 25 °C.

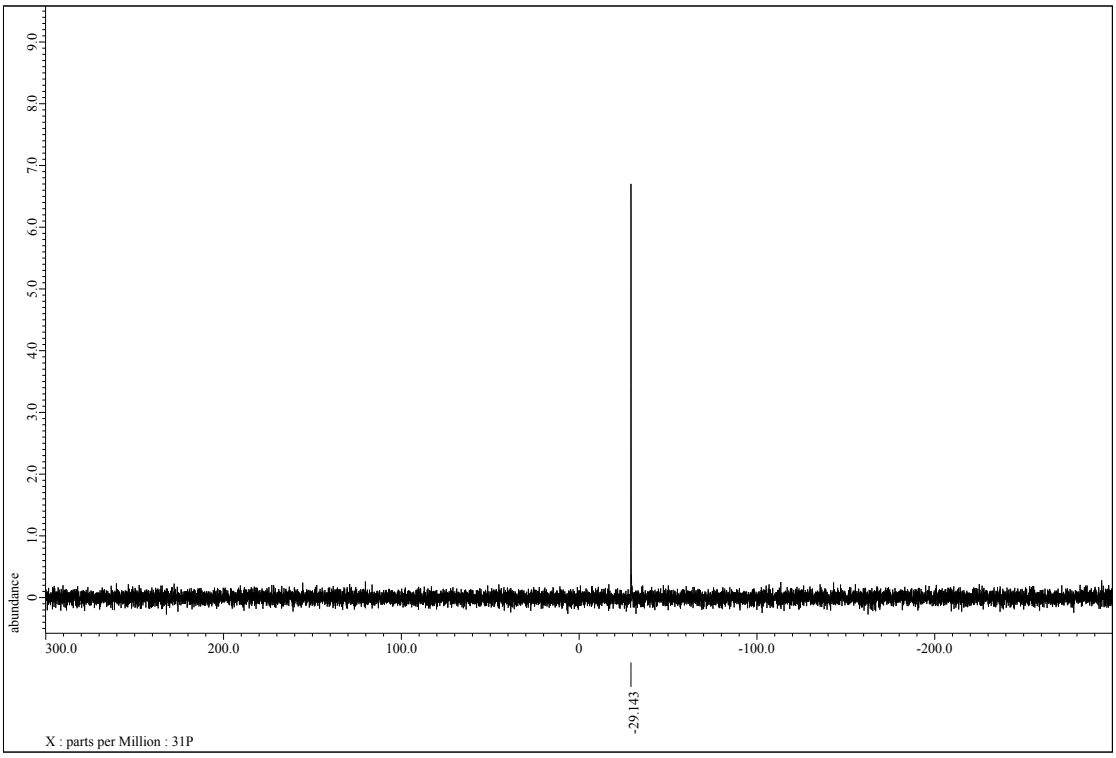

Figure S25. ^{31}P NMR spectrum of **1b** in $CDCl_3$ at 25 °C.

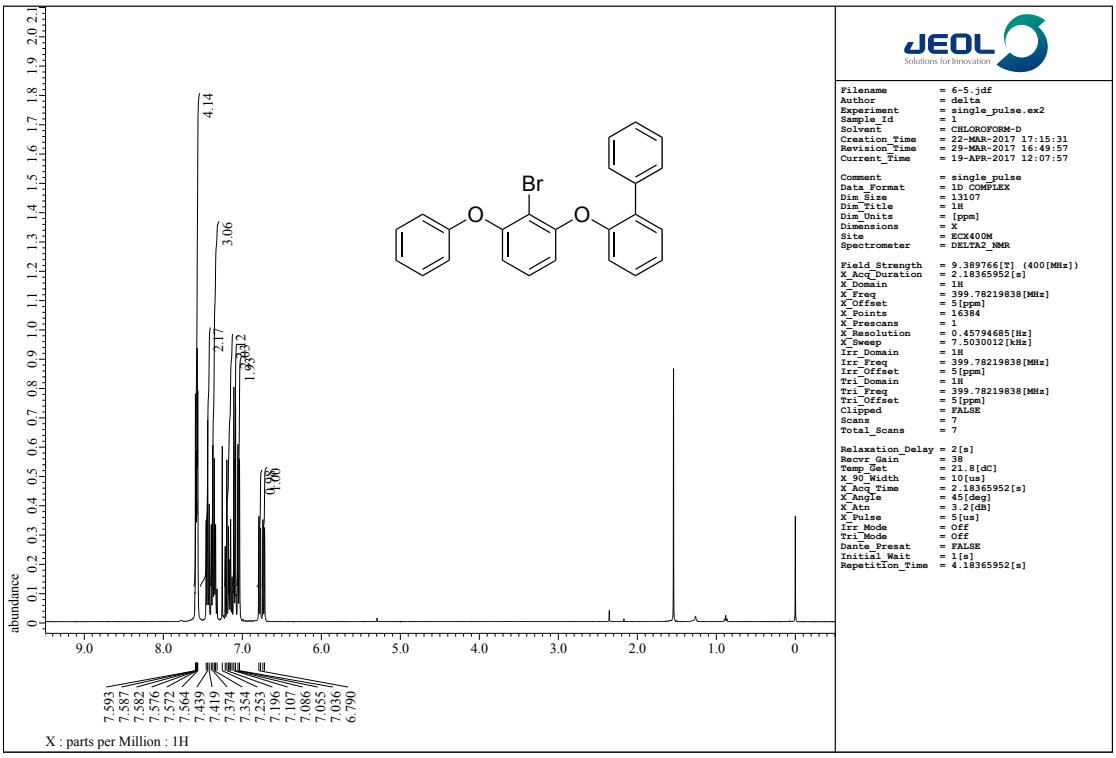

Figure S26. ^{1}H NMR spectrum of **6** in $CDCl_3$ at 25 °C.

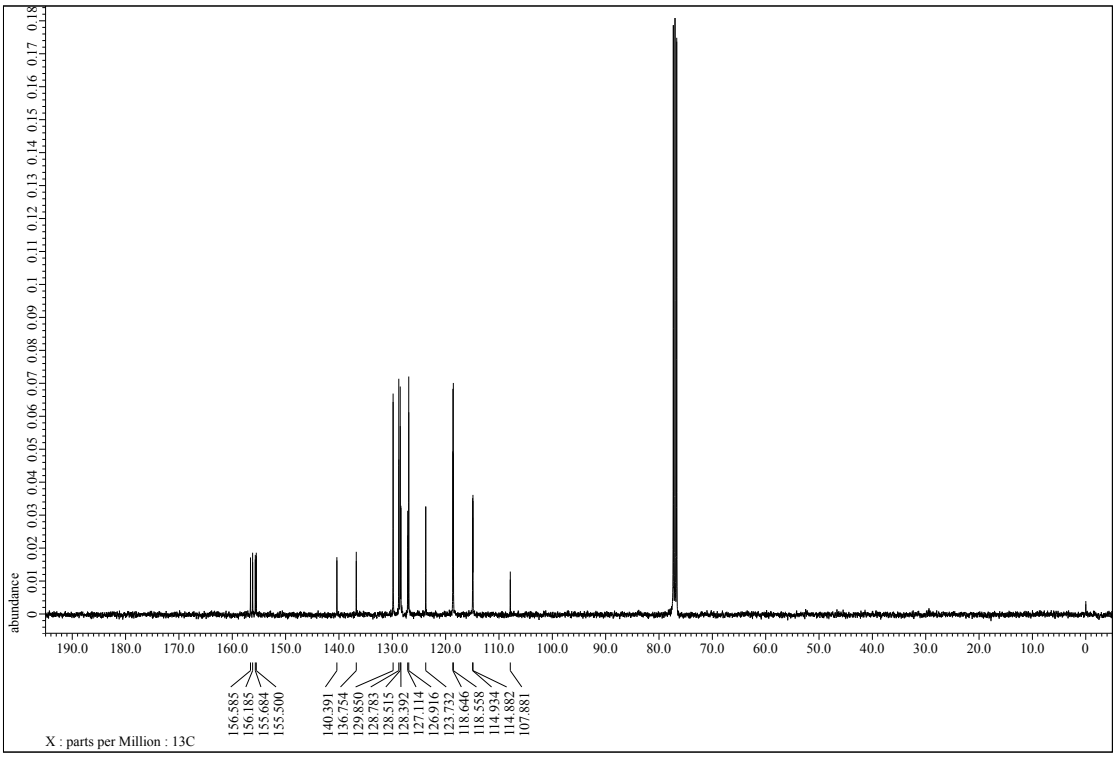

Figure S27. ^{13}C NMR spectrum of **6** in $CDCl_3$ at 25 °C.

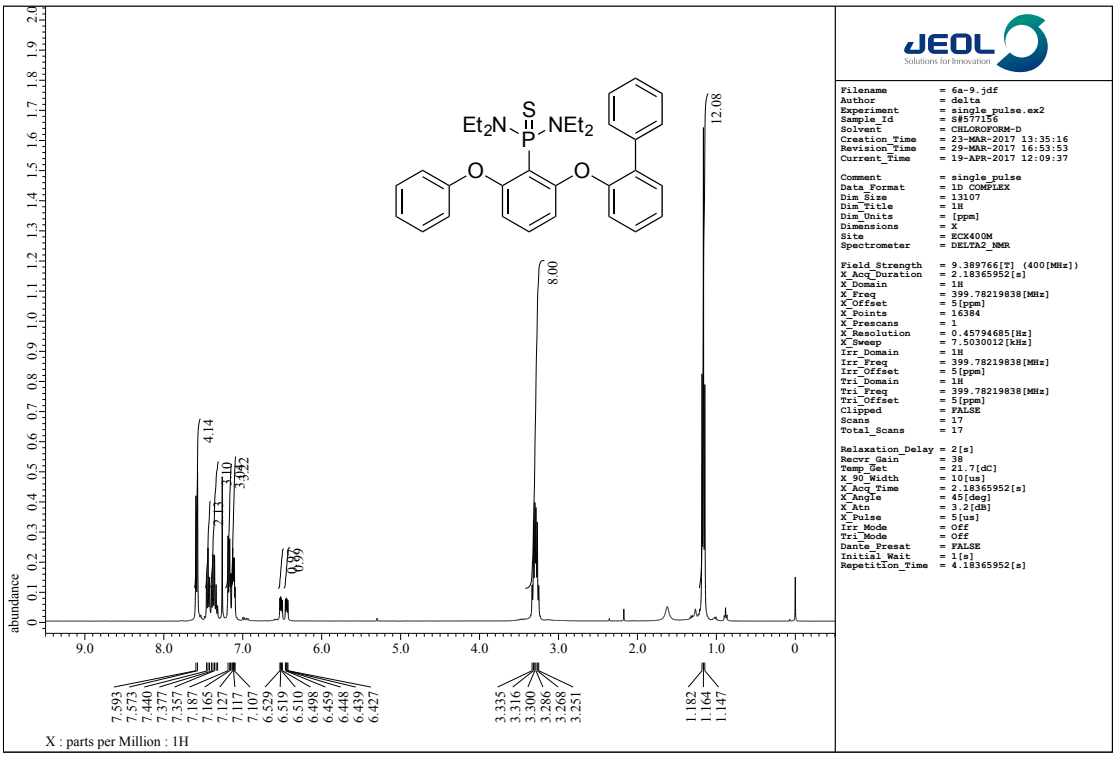

Figure S28. ^{1}H NMR spectrum of **6a** in $CDCl_3$ at 25 °C.

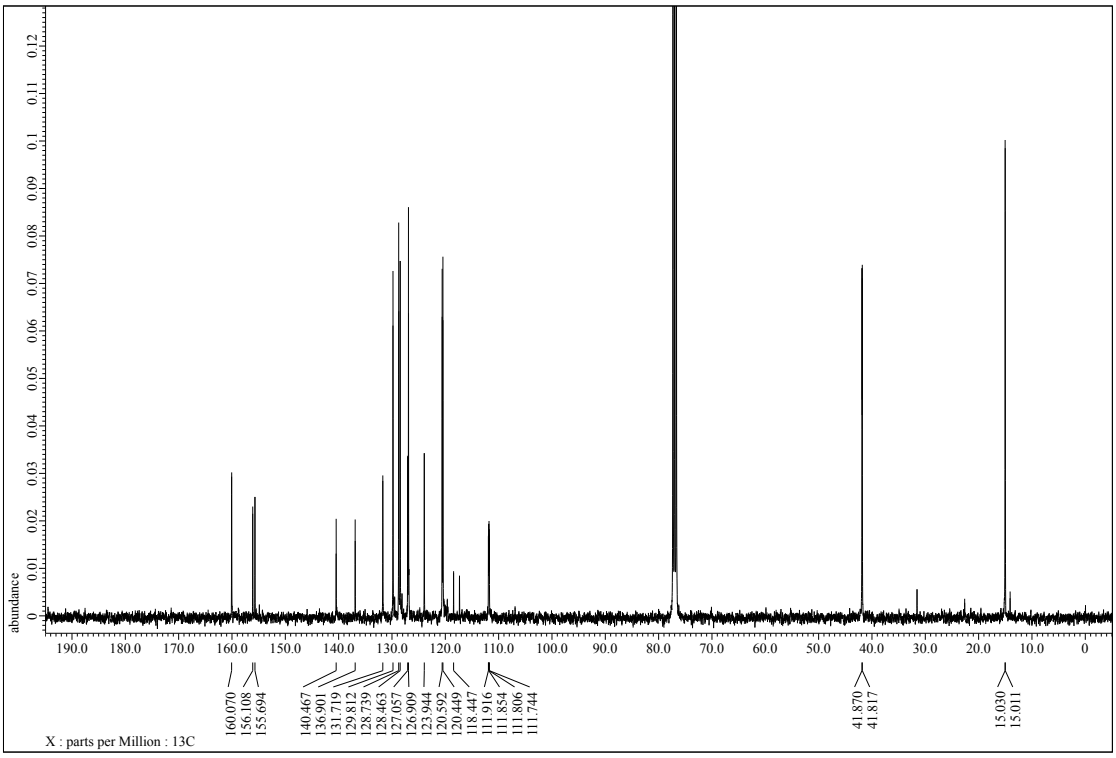

Figure S29. ^{13}C NMR spectrum of **6a** in $CDCl_3$ at 25 °C.

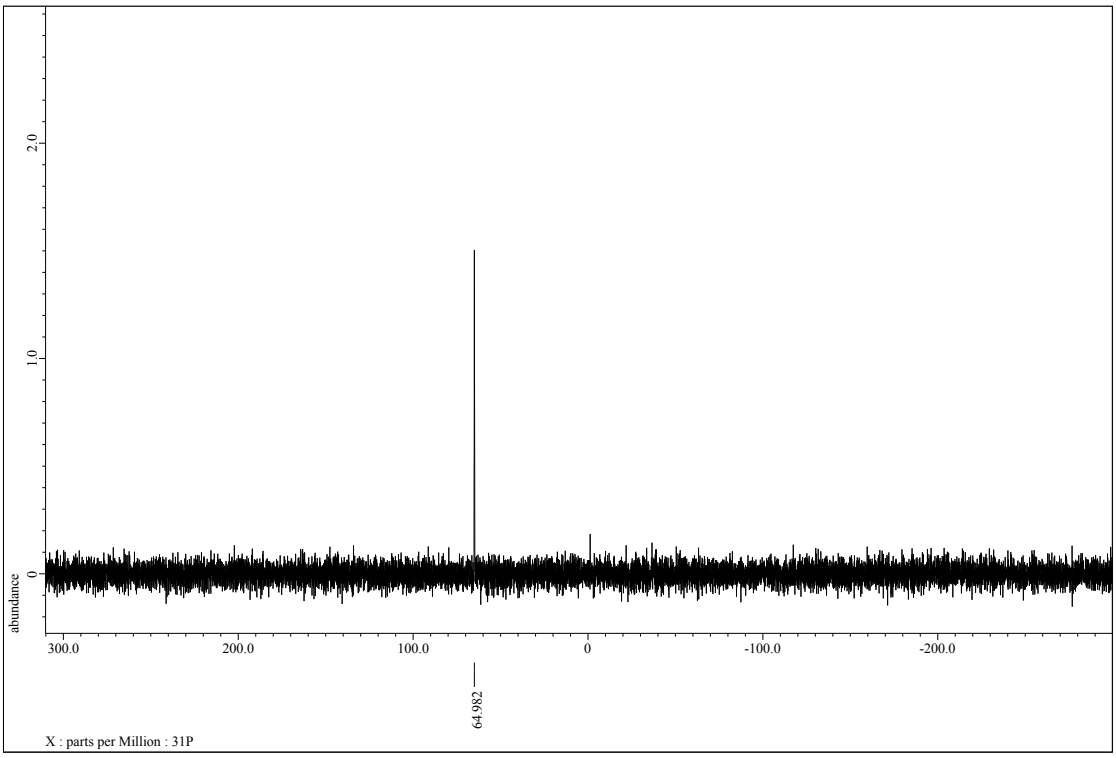

Figure S30. ^{31}P NMR spectrum of **6a** in $CDCl_3$ at 25 °C.

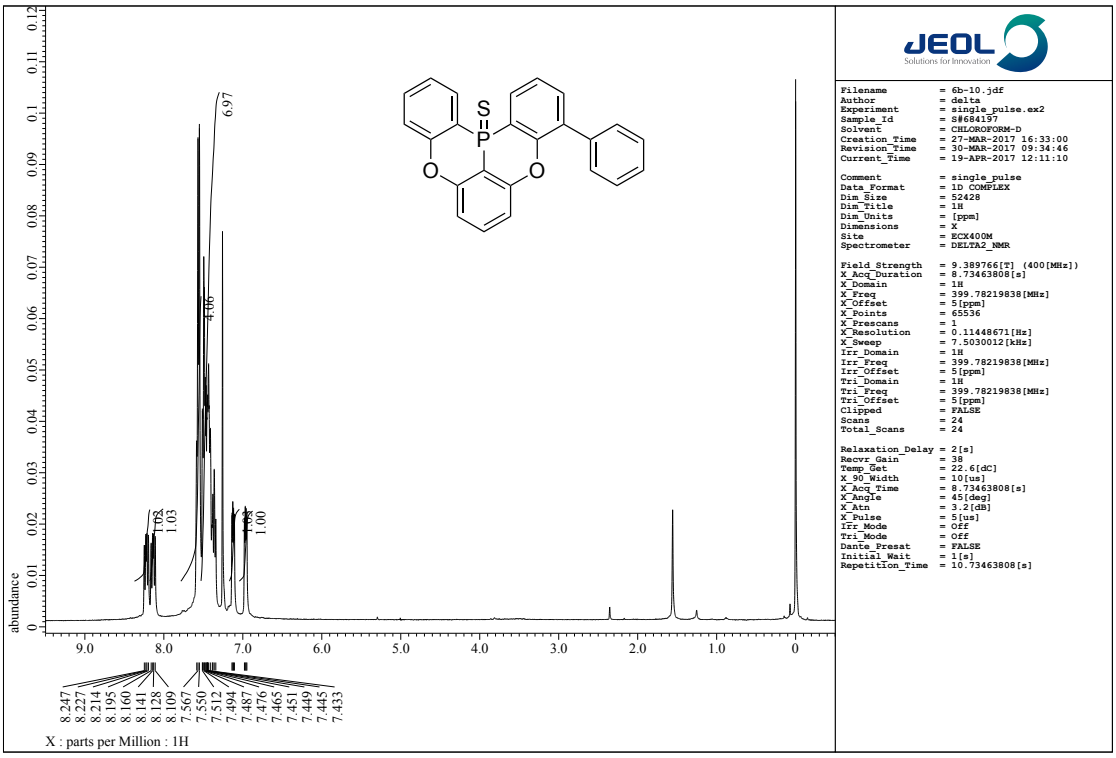

Figure S31. ^{1}H NMR spectrum of **6b** in $CDCl_3$ at 25 °C.

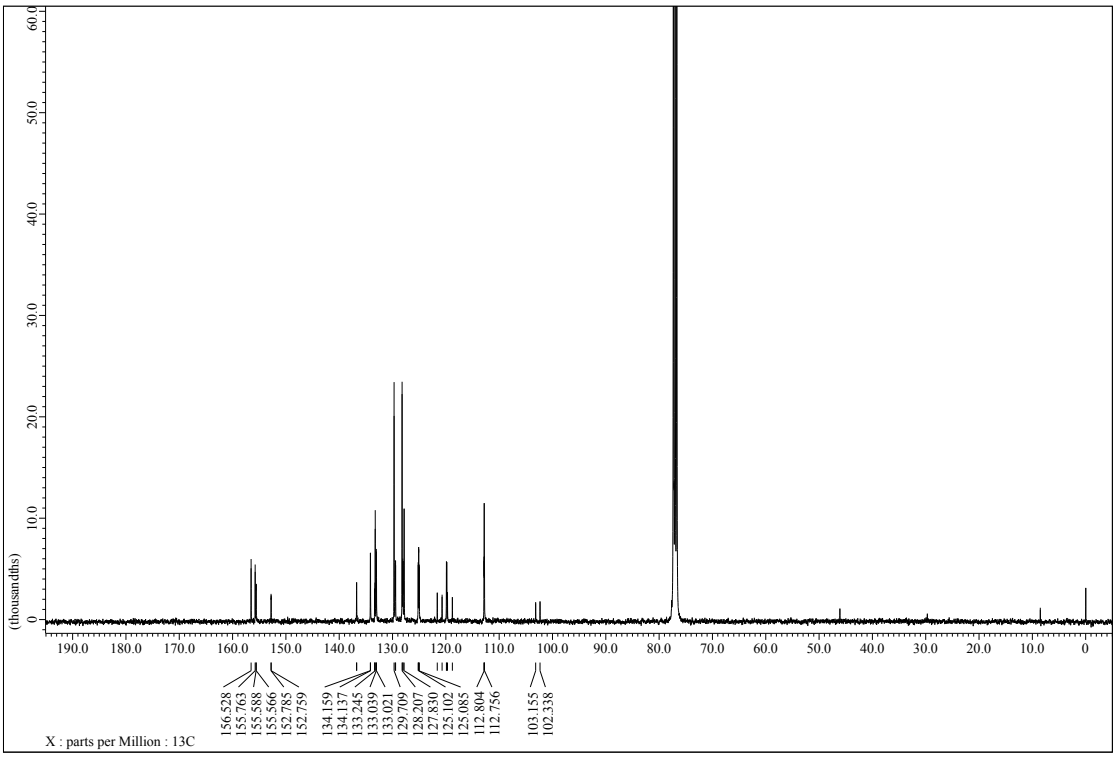

Figure S32. ^{13}C NMR spectrum of **6b** in $CDCl_3$ at 25 °C.

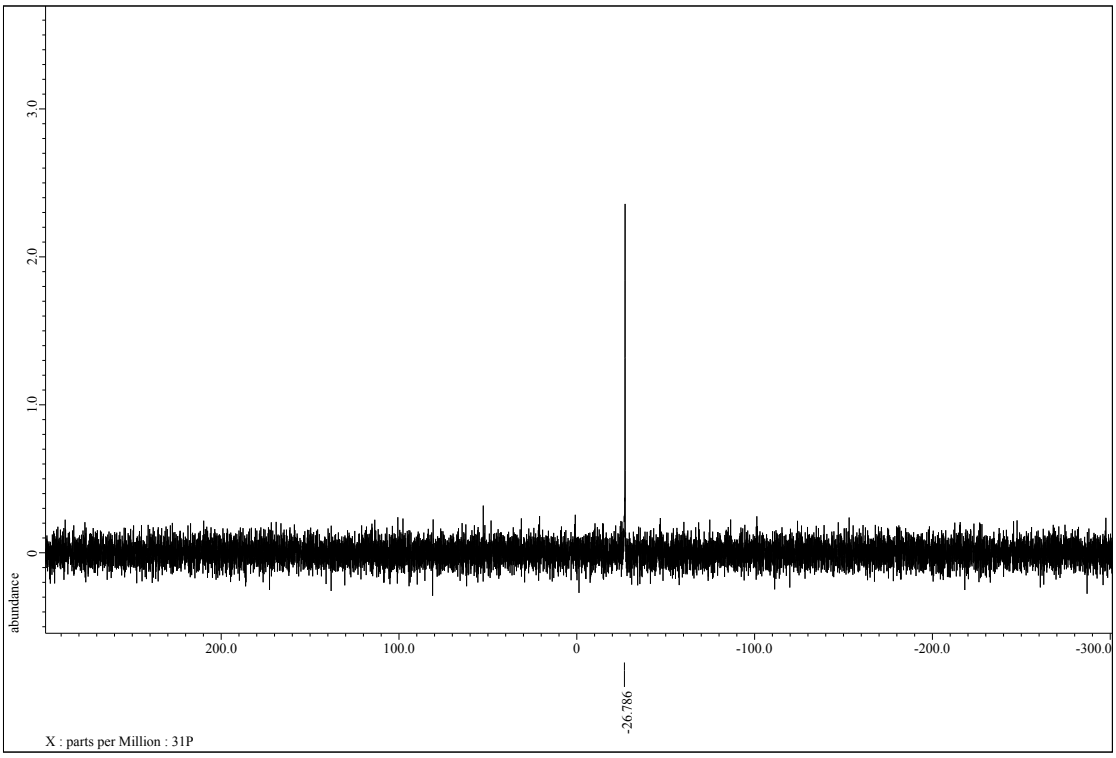

Figure S33. ^{31}P NMR spectrum of **6c** in $CDCl_3$ at 25 °C.

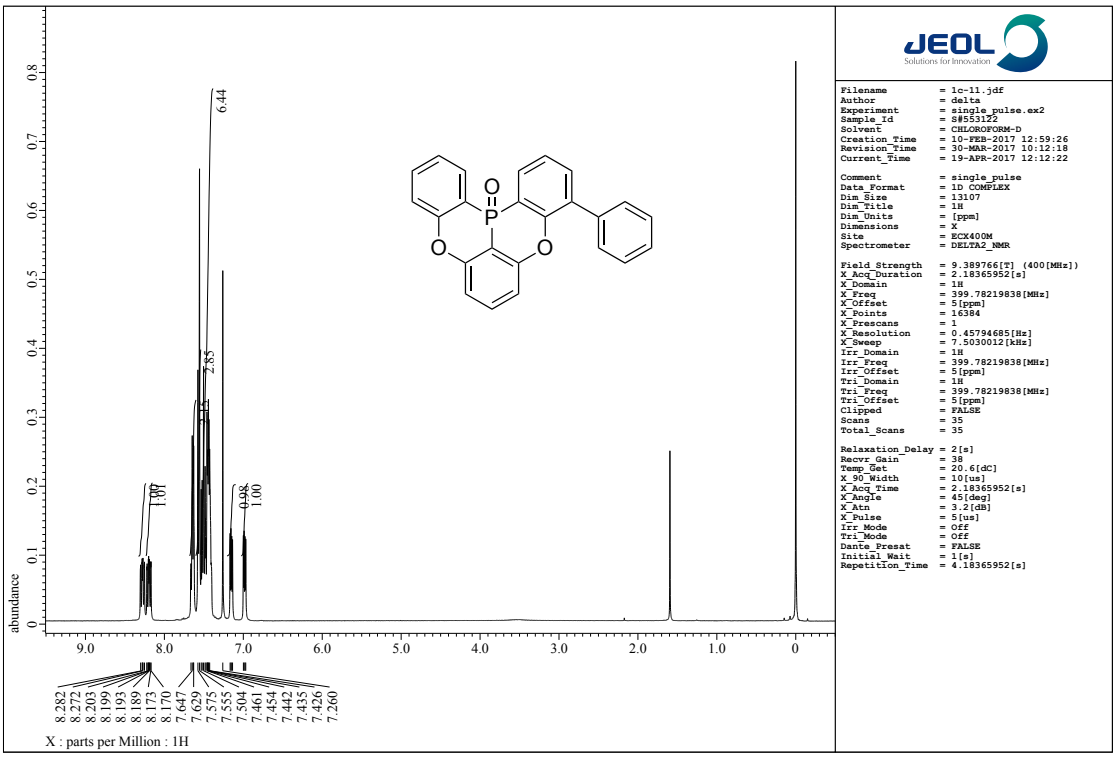

Figure S34. ^{1}H NMR spectrum of **1c** in $CDCl_3$ at 25 °C.

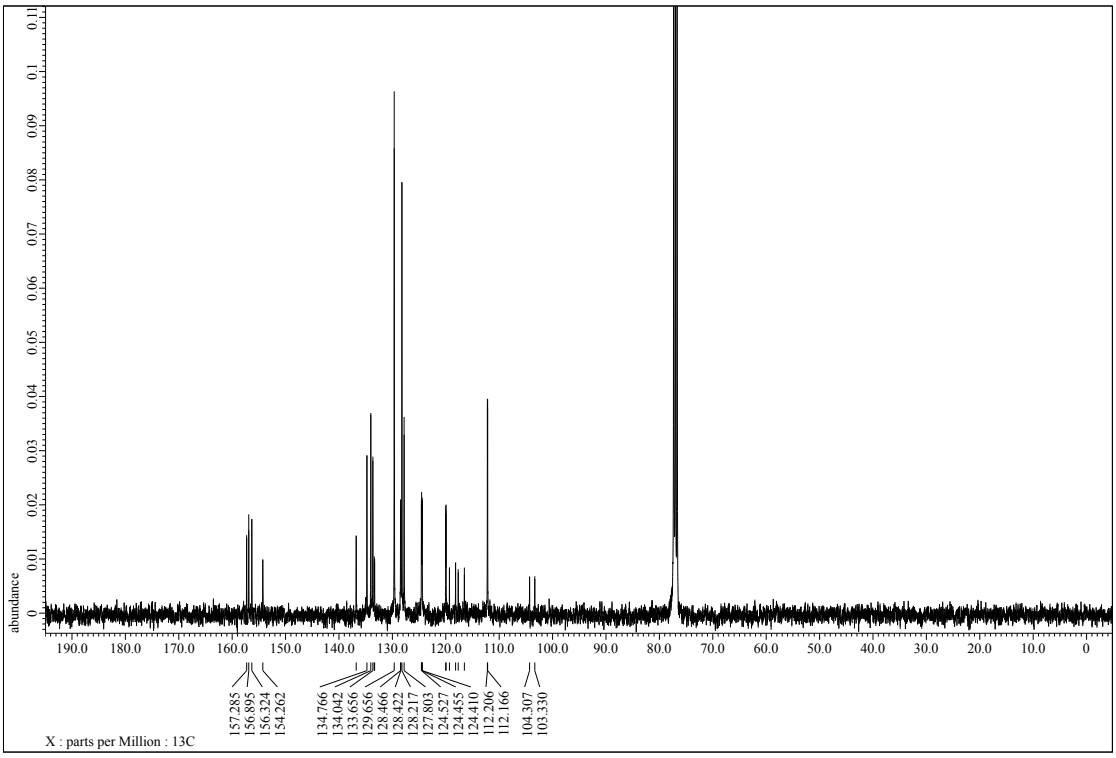

Figure S35. ^{13}C NMR spectrum of **1c** in $CDCl_3$ at 25 °C.

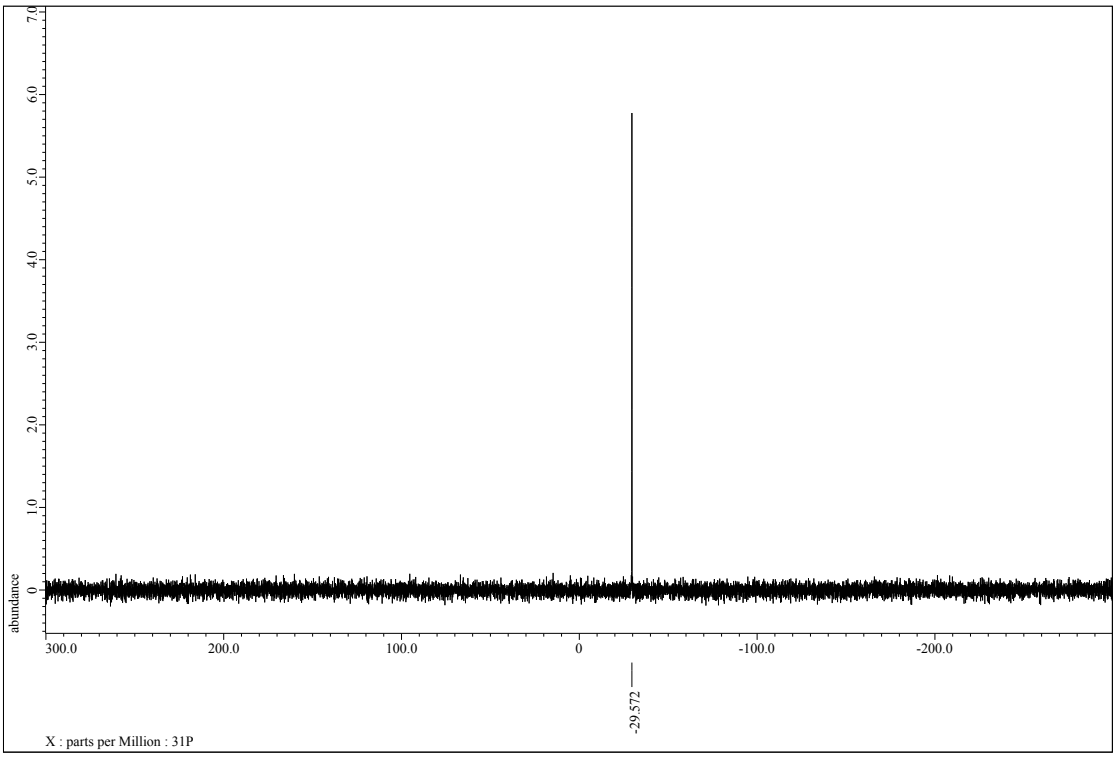

Figure S36. ^{31}P NMR spectrum of **1c** in $CDCl_3$ at 25 °C.